

A quasi-static electromagnetic analysis for experiments with strong permanent magnets

Sven Nordebo, *Senior Member, IEEE*, Alexander Gustafsson

Abstract—An electromagnetic analysis is presented for experiments with strong permanent disc magnets. The analysis is based on the well known experiment that demonstrates the effect of circulating eddy currents by dropping a strong magnet through a vertically placed metal cylinder and observing how the magnet is falling through the cylinder with a constant velocity. A rigorous theory for this phenomenon is provided based on the quasi-static approximation of the Maxwell equations, an infinitely long cylinder (no edge effects) and a constant magnetization of the magnetic disc. The results are useful for teachers and students in electromagnetics who wish to obtain a deeper insight into the analysis and experiments regarding this phenomenon, or with industrial applications such as the calibration of strong permanent magnets, magnetic breaks, conductivity measurements, etc. Several experiments and numerical computations are included to validate and to illustrate the theory.

Index Terms—Neodymium magnets, eddy currents, circulating currents, quasi-static electromagnetic analysis.

I. INTRODUCTION

A well known physics/electromagnetics experiment to demonstrate the effect of circulating eddy currents is to drop a strong magnet through a vertically placed metal cylinder and to observe how the magnet, quite unexpectedly, is not accelerating as usual but is only slowly falling through the cylinder with a constant velocity. The stronger the magnet, or the lower the resistance of the metal cylinder, the slower is the fall through the cylinder. The experiment demonstrates that circulating eddy currents are induced inside the metal cylinder due to the changing magnetic flux, *i.e.*, the Faraday's law of induction, and that these induced currents cause a secondary magnetic field and associated magnetic forces that oppose the fall of the magnet, all in accordance with Lenz's law as well as the Biot-Savart law [2, 6, 7]. Since the magnet (according to the experiment) is falling with a constant velocity, it is immediately realized that the loss in mechanical potential energy of the magnet must be equal to the electrical resistive losses inside the metal cylinder.

This experiment is often conducted at high school level and in basic courses at the universities, etc., and is nowadays readily accessible by everyone due to the availability of cheap super strong neodymium permanent magnets. This type of rare-earth magnets are typically made of an alloy of neodymium, iron and boron ($\text{Nd}_2\text{Fe}_{14}\text{B}$), and the sintered neodymium magnets are currently the most powerful permanent magnets that are commercially available [5]. The

manufacturers grade these magnets in a scale ranging from N35 up to N52 where a higher value indicates a stronger magnet. The super strong neodymium magnets make the experiment quite spectacular together with a thick metal cylinder made of copper or aluminum (or any other non-magnetic and highly conductive material). If the cylinder would be perfectly conducting (super conducting), the magnet would in fact become fixed levitating inside the cylinder. In the laboratory, an efficient way of significantly increasing the conductivity of the cylinder is to cool it down by using liquid nitrogen, or somewhat less spectacular by using dry ice or simply cooling it in a freezer.

This paper provides a rigorous quasi-static electromagnetic analysis for this experiment. The analysis exploits cylindrical symmetries and relies on several well-known properties regarding cylindrical Bessel functions and related Green's function expansions [1, 3, 7, 9, 10], and it provides finally an exact analytical expression for the velocity of the falling magnet. The application of the theory is illustrated by identifying the magnetization of a magnet when the conductivity of the cylinder and the velocity of the fall is known. A validation of the theory is obtained by demonstrating the consistency of this identification based on different measurement cylinders. The application of the theory is also illustrated by estimating the conductivity (and hence the temperature) of the metal cylinders based on different temperature scenarios.

II. ANALYTICAL SOLUTION

A. Problem formulation

A strong cylindrically shaped disc magnet with constant magnetization M [Am^{-1}], mass m [kg], height h [m] and radius a [m] is placed inside a metal cylinder as depicted in Figure 1. It is assumed that the cylinder is infinitely long and hence that edge effects can be neglected. The cylindrical coordinates are denoted (ρ, ϕ, z) and the corresponding unit vectors $(\hat{\rho}, \hat{\phi}, \hat{z})$. The radius vector is $\mathbf{r} = \rho\hat{\rho} + z\hat{z}$. The cartesian coordinates are denoted (x, y, z) and the corresponding unit vectors $(\hat{x}, \hat{y}, \hat{z})$.

The inner radius of the metal cylinder is ρ_1 [m] and the outer radius ρ_2 [m], and the conductivity of the metal is σ [Sm^{-1}]. The electromagnetic response of the magnet is neglected (the relative permittivity and permeability are assumed to be $\epsilon = \mu = 1$), except that it exhibits a very strong constant magnetization (dipole moment per unit volume) with a magnetization vector $\mathbf{M} = M\hat{z}$. It is observed that this situation is equivalent to placing a cylindrically shaped sheet surface current in vacuum having a current density $\mathbf{J}_s = -\hat{\rho} \times \mathbf{M} = M\hat{\phi}$ at the corresponding magnet surface at radius a , and that there are

Manuscript received December 3, 2024. The authors acknowledge the constructive criticism provided by Patrik Wahlberg.

Sven Nordebo and Alexander Gustafsson are with the Department of Physics and Electrical Engineering, Linnaeus University, 351 95 Växjö, Sweden. (E-mail: {sven.nordebo,alexander.gustafsson}@lnu.se).

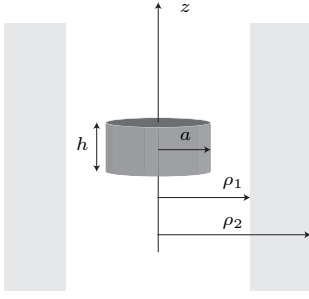


Fig. 1. Geometry of the problem.

no other equivalent currents emanating from the top or bottom of the magnet, see *e.g.*, [2, 6, 7].

The magnet is placed in a gravity field and experiences the force $-mg\hat{z}$ where $g = 9.81 \text{ ms}^{-2}$. The position of the center of the magnet is denoted $z_0(t)$ where t is the time. The magnet is released at $t = 0$ with initial position $z_0(0) = 0$ and velocity $\dot{z}_0(0) = 0$, and where the dot denotes a differentiation with respect to the time. The motion of the magnet will be determined for $t \geq 0$.

B. The quasi-static approximation

Let $\mathbf{E}(\mathbf{r}, t)$, $\mathbf{D}(\mathbf{r}, t)$, $\mathbf{H}(\mathbf{r}, t)$, $\mathbf{B}(\mathbf{r}, t)$ and $\mathbf{J}(\mathbf{r}, t)$ denote the electric field intensity, the electric flux density, the magnetic field intensity, the magnetic flux density and the electric current density, respectively, see *e.g.*, [2, 6, 7]. Maxwell's equations under the quasi-static approximation is given by

$$\begin{cases} \nabla \times \mathbf{E}(\mathbf{r}, t) = -\frac{\partial}{\partial t} \mathbf{B}(\mathbf{r}, t), \\ \nabla \times \mathbf{H}(\mathbf{r}, t) = \mathbf{J}(\mathbf{r}, t), \end{cases} \quad (1)$$

where the displacement current $\frac{\partial}{\partial t} \mathbf{D}(\mathbf{r}, t)$ is neglected, leading to a diffusion equation where there are no retarded potentials and no wave propagation phenomena [7]. The approximation can be justified by the fact that the magnet is very strong, and hence that the effect of the current source \mathbf{J} will dominate over the effect of the displacement current $\frac{\partial}{\partial t} \mathbf{D}(\mathbf{r}, t)$. To see this, consider a conductive material with real relative permittivity ϵ_r , conductivity σ and displacement current

$$\frac{\partial}{\partial t} \mathbf{D}(\mathbf{r}, t) = \epsilon_0 \epsilon_r \frac{\partial}{\partial t} \mathbf{E}(\mathbf{r}, t) + \sigma \mathbf{E}(\mathbf{r}, t). \quad (2)$$

As the magnet is getting stronger (M is getting larger) a smaller induced current inside the cylinder will be required to oppose the acceleration. Hence, as M is getting larger, the source term $\mathbf{J}(\mathbf{r}, t)$ in (1) above will increase at the same rate as the induced current $\sigma \mathbf{E}(\mathbf{r}, t)$ will decrease.

C. Ampère's current law

The first step is to determine the magnetic field of the permanent magnet when it is at rest at $z = 0$. Here, the source consists of a cylindrically shaped sheet surface current with current density $\mathbf{J}_s = -\hat{\rho} \times \mathbf{M} = M\hat{\phi}$ at the surface of the magnet at radius a . The magnetic potential is hence given by

$$\mathbf{A}(\mathbf{r}) = \mu_0 \int_0^{2\pi} \int_{-h/2}^{h/2} \frac{1}{4\pi|\mathbf{r} - \mathbf{r}'|} \mathbf{J}_s(\mathbf{r}') dS', \quad (3)$$

where $\mu_0 = 4\pi \cdot 10^{-7} \text{ Hm}^{-1}$ is the permeability of vacuum, $\mathbf{J}_s(\mathbf{r}') = M\hat{\phi}'$ and $dS' = a d\phi' dz'$, *cf.*, *e.g.*, [2, 6, 7].

The field $\mathbf{A}(\mathbf{r})$ is then evaluated in the x - z plane where $\phi = 0$, and adequate symmetries are exploited to yield

$$\mathbf{A}(\mathbf{r}) = \mu_0 a M \hat{\phi} \int_0^{2\pi} \int_{-h/2}^{h/2} \frac{1}{4\pi|\mathbf{r} - \mathbf{r}'|} \cos \phi' d\phi' dz', \quad (4)$$

where $\mathbf{A}(\mathbf{r})$ is axial-symmetric (A_ϕ is independent of ϕ), $\hat{\phi}' = -\hat{x} \sin \phi' + \hat{y} \cos \phi'$, and in the x - z plane the Green's function $1/4\pi|\mathbf{r} - \mathbf{r}'|$ is even in ϕ' and $\hat{y} = \hat{\phi}$.

Next, the free space Green's function is expanded in cylindrical Bessel functions as

$$\frac{1}{4\pi|\mathbf{r} - \mathbf{r}'|} = \frac{i}{8\pi} \int_{-\infty}^{\infty} \sum_{m=-\infty}^{\infty} J_m(i|\alpha|\rho_{<}) H_m^{(1)}(i|\alpha|\rho_{>}) e^{im(\phi - \phi')} e^{i\alpha(z - z')} d\alpha, \quad (5)$$

see *e.g.*, [1, 3, 7] and Appendix A. Here, $J_m(\cdot)$ and $H_m^{(1)}(\cdot)$ are the regular Bessel functions and the Hankel functions of the first kind, respectively, both of order m , see *e.g.*, [1, 7, 9, 10]. The arguments above are defined by $\rho_{<} = \min\{\rho, \rho'\}$ and $\rho_{>} = \max\{\rho, \rho'\}$, and the integration variable α is a real valued Fourier variable corresponding to a Fourier transformation along the longitudinal coordinate z .

By inserting (5) into (4) and integrating over the ϕ' and z' coordinates, the magnetic potential is given by

$$\mathbf{A}(\mathbf{r}) = \mu_0 a h M \hat{\phi} \frac{i}{4} \int_{-\infty}^{\infty} J_1(i|\alpha|\rho_{<}) H_1^{(1)}(i|\alpha|\rho_{>}) \frac{\sin(\alpha h/2)}{\alpha h/2} e^{i\alpha z} d\alpha, \quad (6)$$

where $\rho' = a$, and where the following integrals have been used

$$\begin{cases} \int_0^{2\pi} e^{-im\phi'} \cos \phi' d\phi' = \pi(\delta_{m,1} + \delta_{m,-1}), \\ \int_{-h/2}^{h/2} e^{-i\alpha z'} dz' = h \frac{\sin(\alpha h/2)}{\alpha h/2}, \end{cases} \quad (7)$$

where $\delta_{m,n}$ denotes the Kronecker delta [1], and where the relations $C_{-m}(\zeta) = (-1)^m C_m(\zeta)$ have been used which are valid for any cylinder function of order m [9].

The magnetic flux density is given by $\mathbf{B} = \nabla \times \mathbf{A}$, and in cylindrical coordinates

$$B_z(\rho, z) = \frac{1}{\rho} \frac{\partial}{\partial \rho} \rho A_\phi(\rho, z). \quad (8)$$

The following explicit results are obtained

$$B_z^{(1)}(\rho, z) = \mu_0 a h M \frac{i}{4} \int_{-\infty}^{\infty} \frac{1}{\rho} \frac{\partial}{\partial \rho} \rho J_1(i|\alpha|\rho) H_1^{(1)}(i|\alpha|a) \frac{\sin(\alpha h/2)}{\alpha h/2} e^{i\alpha z} d\alpha, \quad (9)$$

where $\rho < \rho' = a$, and

$$B_z^{(2)}(\rho, z) = \mu_0 a h M \frac{i}{4} \int_{-\infty}^{\infty} \frac{1}{\rho} \frac{\partial}{\partial \rho} \rho H_1^{(1)}(i|\alpha|\rho) J_1(i|\alpha|a) \frac{\sin(\alpha h/2)}{\alpha h/2} e^{i\alpha z} d\alpha, \quad (10)$$

where $\rho > \rho' = a$. The total flux in the z -direction through a circular surface parallel to the x - y plane with radius $\rho > a$ and with its center positioned at height z (and $x = y = 0$), is given by

$$\begin{aligned} \Phi(\rho, z) &= \int_0^a \int_0^{2\pi} B_z^{(1)}(\rho', z) \rho' d\rho' d\phi' \\ &+ \int_a^\rho \int_0^{2\pi} B_z^{(2)}(\rho', z) \rho' d\rho' d\phi' = \int_{-\infty}^\infty F(\alpha, \rho) e^{i\alpha z} d\alpha, \end{aligned} \quad (11)$$

where

$$F(\alpha, \rho) = \mu_0 a h M \frac{\pi}{2} \rho H_1^{(1)}(i|\alpha|\rho) i J_1(i|\alpha|a) \frac{\sin(\alpha h/2)}{\alpha h/2}. \quad (12)$$

The functions $H_1^{(1)}(i|\alpha|\rho)$ and $i J_1(i|\alpha|a)$ are real valued (see the next section), and hence the function $F(\alpha, \rho)$ is real valued and even in the variable α .

D. Computational issues and asymptotics of integrands

For computational purposes it is useful to employ the regular and the singular modified Bessel functions $I_m(\zeta)$ and $K_m(\zeta)$, respectively, which are defined by

$$\begin{cases} I_m(\zeta) = i^{-m} J_m(i\zeta), \\ K_m(\zeta) = i^{m+1} \frac{\pi}{2} H_m^{(1)}(i\zeta), \end{cases} \quad (13)$$

and which are real valued for real arguments ζ , see [1, 9]. For analysis purposes it is also useful to employ the following small argument asymptotics

$$\begin{cases} J_m(\zeta) \sim \frac{1}{m!} \left(\frac{\zeta}{2}\right)^m, \\ H_0^{(1)}(\zeta) \sim i \frac{2}{\pi} \ln \frac{\zeta}{2}, \\ H_m^{(1)}(\zeta) \sim \frac{-i(m-1)!}{\pi} \left(\frac{2}{\zeta}\right)^m, \end{cases} \quad \begin{cases} I_m(\zeta) \sim \frac{1}{m!} \left(\frac{\zeta}{2}\right)^m, \\ K_0(\zeta) \sim -\ln \frac{i\zeta}{2}, \\ K_m(\zeta) \sim \frac{(m-1)!}{2} \left(\frac{2}{\zeta}\right)^m, \end{cases} \quad (14)$$

as $\zeta \rightarrow 0$, where $m \geq 0$ in the first line above and $m \geq 1$ in the third, cf., [1, 9].

To compute the magnetic flux density $B_z(\rho, z)$ for $\rho = 0$ and $z = 0$ based on (9), it is noted that the term $\frac{1}{\rho} \frac{\partial}{\partial \rho} \rho J_1(i|\alpha|\rho) \sim i|\alpha|$ as $\rho \rightarrow 0$, and hence that

$$B_z(0, 0) = \mu_0 a h M \frac{1}{\pi} \int_0^\infty \alpha K_1(\alpha a) \frac{\sin(\alpha h/2)}{\alpha h/2} d\alpha, \quad (15)$$

where (13) has been used, as well as the fact that the integrand is even. By using (14), it is seen that the integrand in (15) approaches the value $1/a$ as $\alpha \rightarrow 0$.

The large argument asymptotics of the regular Bessel functions and of the Hankel functions of the first kind are given by

$$\begin{cases} J_m(\zeta) \sim \sqrt{\frac{2}{\pi\zeta}} \cos(\zeta - \frac{1}{2}m\pi - \frac{1}{4}\pi), \\ H_m^{(1)}(\zeta) \sim \sqrt{\frac{2}{\pi\zeta}} e^{i(\zeta - \frac{1}{2}m\pi - \frac{1}{4}\pi)} \left(1 + i \frac{4m^2 - 1}{8\zeta}\right), \end{cases} \quad (16)$$

as $\zeta \rightarrow \infty$, see [1, 9]. Hence, for large α it is concluded that the integrand in (15) decays with an exponential factor $e^{-\alpha a}$ as $\alpha \rightarrow \infty$.

E. Faraday's law of induction

The integral form of Faraday's law of induction [2, 6, 7] is given by

$$\int_C \mathbf{E}(\mathbf{r}, t) \cdot d\mathbf{r} = \int_S -\frac{\partial}{\partial t} \mathbf{B}(\mathbf{r}, t) \cdot d\mathbf{S}, \quad (17)$$

where S is the circular surface with radius ρ positioned at height z and C its (right-handed) contour. The quasi-static approximation is now incorporated by letting $\Phi(\rho, z - z_0(t))$ describe the magnetic flux of the moving magnet at position $z_0(t)$ and where $\Phi(\rho, \cdot)$ is given by (11). By further exploiting the axial symmetries using $\mathbf{E}(\mathbf{r}, t) = \hat{\phi} E_\phi(\rho, z, t)$, the Faraday's law of induction yields

$$\begin{aligned} E_\phi(\rho, z, t) 2\pi\rho &= -\frac{\partial}{\partial t} \Phi(\rho, z - z_0(t)) \\ &= -\frac{\partial}{\partial t} \int_{-\infty}^\infty F(\alpha, \rho) e^{i\alpha(z - z_0(t))} d\alpha, \end{aligned} \quad (18)$$

or

$$E_\phi(\rho, z, t) = \frac{\dot{z}_0(t)}{2\pi\rho} \int_{-\infty}^\infty i\alpha F(\alpha, \rho) e^{i\alpha(z - z_0(t))} d\alpha. \quad (19)$$

The induced current density is obtained as

$$J_\phi(\rho, z, t) = \sigma E_\phi(\rho, z, t), \quad (20)$$

and it is noted that $J_\phi(\rho, z, t)$ is a real valued function that is odd in the variable $z - z_0(t)$. Hence, the induced current is circulating in opposite directions above and below the center of the magnet, all in accordance with Lenz's law [2, 6, 7].

The total induced current for $z > z_0(t)$ is given by

$$\begin{aligned} I_{\text{ind}} &= \int_{\rho_1}^{\rho_2} \int_{z_0(t)}^\infty J_\phi(\rho, z, t) d\rho dz \\ &= \sigma \frac{\dot{z}_0(t)}{2\pi} \int_{-\infty}^\infty i\alpha \int_{\rho_1}^{\rho_2} \frac{1}{\rho} F(\alpha, \rho) d\rho \int_0^\infty e^{i\alpha z} dz d\alpha \\ &= \sigma \frac{\dot{z}_0(t)}{4} \mu_0 a h M \int_{-\infty}^\infty \frac{1}{|\alpha|} \frac{\sin(\alpha h/2)}{\alpha h/2} J_1(i|\alpha|a) \\ &\quad \left(H_0^{(1)}(i|\alpha|\rho_2) - H_0^{(1)}(i|\alpha|\rho_1) \right) d\alpha. \end{aligned} \quad (21)$$

The relation (12) was used in the derivation above, as well as the identity $H_1^{(1)}(\zeta) = -\frac{\partial}{\partial \zeta} H_0^{(1)}(\zeta)$, and the Fourier integral

$$\int_0^\infty e^{i\alpha z} dz = \frac{1}{-i\alpha} + \pi\delta(\alpha), \quad (22)$$

which should be interpreted in the sense of distributions [11].

By using the modified Bessel functions defined in (13), the total induced current (21) can also be written

$$\begin{aligned} I_{\text{ind}} &= \sigma \dot{z}_0(t) \mu_0 a h M \frac{1}{\pi} \int_0^\infty \frac{1}{\alpha} \frac{\sin(\alpha h/2)}{\alpha h/2} I_1(\alpha a) \\ &\quad (K_0(\alpha\rho_2) - K_0(\alpha\rho_1)) d\alpha. \end{aligned} \quad (23)$$

F. Power loss and the velocity of the fall

The resistive power loss in the metal can be computed based on Poyntings theorem [7] as

$$P_{\text{loss}}(t) = \sigma \int_{\rho_1}^{\rho_2} \int_0^{2\pi} \int_{-\infty}^{\infty} |E_\phi(\rho, z, t)|^2 \rho d\rho d\phi dz, \quad (24)$$

where $E_\phi(\rho, z, t)$ is given by (19). It follows that

$$\begin{aligned} P_{\text{loss}}(t) &= \sigma 2\pi \int_{\rho_1}^{\rho_2} \int_{-\infty}^{\infty} \left(\frac{\dot{z}_0(t)}{2\pi\rho} \right)^2 \int_{-\infty}^{\infty} i\alpha F(\alpha, \rho) e^{i\alpha(z-z_0(t))} d\alpha \\ &\quad \int_{-\infty}^{\infty} -i\alpha' F(\alpha', \rho) e^{-i\alpha'(z-z_0(t))} d\alpha' \rho d\rho dz \\ &= \sigma 2\pi \int_{\rho_1}^{\rho_2} \left(\frac{\dot{z}_0(t)}{2\pi\rho} \right)^2 \int_{-\infty}^{\infty} \int_{-\infty}^{\infty} \alpha F(\alpha, \rho) \\ &\quad \alpha' F(\alpha', \rho) \int_{-\infty}^{\infty} e^{i(\alpha-\alpha')(z-z_0(t))} dz d\alpha d\alpha' \rho d\rho \\ &= \sigma \dot{z}_0^2(t) \int_{-\infty}^{\infty} \int_{\rho_1}^{\rho_2} \frac{1}{\rho^2} \alpha^2 F^2(\alpha, \rho) \rho d\rho d\alpha, \quad (25) \end{aligned}$$

where the distributional relation $\int_{-\infty}^{\infty} e^{i(\alpha-\alpha')(z-z_0(t))} dz = 2\pi\delta(\alpha-\alpha')$ has been used. By inserting (12) into the last line above, the following result is obtained

$$P_{\text{loss}}(t) = \sigma M^2 \dot{z}_0^2(t) \mu_0^2 C, \quad (26)$$

where C (in units $[m^3]$) is a structure constant that depends on the geometrical parameters (a, h, ρ_1, ρ_2) and which is explicitly given by

$$C = a^2 h^2 \frac{\pi^2}{4} \int_{-\infty}^{\infty} \alpha^2 \frac{\sin^2(\alpha h/2)}{(\alpha h/2)^2} |J_1(i|\alpha|a)|^2 \int_{\rho_1}^{\rho_2} (H_1^{(1)}(i|\alpha|\rho))^2 \rho d\rho d\alpha. \quad (27)$$

The inner integral can be computed explicitly by use of the so called Lommel integral [1, 9, 10] yielding

$$\begin{aligned} &\int_{\rho_1}^{\rho_2} (H_1^{(1)}(i|\alpha|\rho))^2 \rho d\rho \\ &= \frac{1}{2} \rho_2^2 \left[(H_1^{(1)}(i|\alpha|\rho_2))^2 - H_0^{(1)}(i|\alpha|\rho_2) H_2^{(1)}(i|\alpha|\rho_2) \right] \\ &- \frac{1}{2} \rho_1^2 \left[(H_1^{(1)}(i|\alpha|\rho_1))^2 - H_0^{(1)}(i|\alpha|\rho_1) H_2^{(1)}(i|\alpha|\rho_1) \right]. \quad (28) \end{aligned}$$

For computational purposes it is adequate to employ the modified Bessel functions defined in (13), yielding

$$C = a^2 h^2 \int_0^{\infty} \alpha^2 \frac{\sin^2(\alpha h/2)}{(\alpha h/2)^2} I_1^2(\alpha a) 2 \frac{\pi^2}{4} \int_{\rho_1}^{\rho_2} (H_1^{(1)}(i\alpha\rho))^2 \rho d\rho d\alpha, \quad (29)$$

where

$$\begin{aligned} &2 \frac{\pi^2}{4} \int_{\rho_1}^{\rho_2} (H_1^{(1)}(i\alpha\rho))^2 \rho d\rho \\ &= \rho_2^2 \left[(K_1(\alpha\rho_2))^2 - K_0(\alpha\rho_2) K_2(\alpha\rho_2) \right] \\ &- \rho_1^2 \left[(K_1(\alpha\rho_1))^2 - K_0(\alpha\rho_1) K_2(\alpha\rho_1) \right]. \quad (30) \end{aligned}$$

By using (14), it is seen that the integrand in (29) approaches the value 0 as $\alpha \rightarrow 0$. For large α , (13) and (16) are used to conclude that the integrand in (29) decays with a dominating exponential factor $e^{-2\alpha(\rho_1-a)}$ as $\alpha \rightarrow \infty$.

Experiments show that the magnet very quickly assumes a constant velocity as it falls through the metal cylinder. When there is a constant velocity v there is no power exchange associated with an acceleration of the magnet, and all the resistive losses must be attributed to the loss in mechanical potential energy. This gives the power balance equation

$$\sigma M^2 v^2 \mu_0^2 C = -mgv, \quad (31)$$

yielding the simple physical law for stationary motion

$$\sigma M^2 v = -\frac{mg}{\mu_0^2 C}. \quad (32)$$

The resulting velocity v given by (32) can now be inserted into (23) to yield the total induced current

$$I_{\text{ind}} = -\frac{mga h}{\mu_0 M C} \frac{1}{\pi} \int_0^{\infty} \frac{1}{\alpha} \frac{\sin(\alpha h/2)}{\alpha h/2} I_1(\alpha a) (K_0(\alpha\rho_2) - K_0(\alpha\rho_1)) d\alpha. \quad (33)$$

It is noted that the induced current in (33) is independent of the conductivity σ , as expected. The integrand in (33) approaches the value $-(a/2) \ln(\rho_2/\rho_1)$ as $\alpha \rightarrow 0$, and for large α the integrand decays with a dominating exponential factor $e^{-\alpha(\rho_1-a)}$ as $\alpha \rightarrow \infty$.

G. Equation of motion

To determine the motion of the falling magnet the induced magnetic reaction forces acting on the magnet must be derived. Hence, the induced magnetic potential is calculated from the induced current $J_\phi(\rho, z, t)$ as

$$\begin{aligned} \mathbf{A}^{\text{ind}}(\mathbf{r}, t) &= \mu_0 \int_{\rho_1}^{\rho_2} \int_0^{2\pi} \int_{-\infty}^{\infty} \\ &\quad \frac{1}{4\pi|\mathbf{r} - \mathbf{r}'|} J_\phi(\rho', z', t) \hat{\phi}' \rho' d\rho' d\phi' dz'. \quad (34) \end{aligned}$$

The field $\mathbf{A}^{\text{ind}}(\mathbf{r}, t)$ is then evaluated in the x - z plane where $\phi = 0$, and adequate symmetries are exploited to yield

$$\begin{aligned} \mathbf{A}^{\text{ind}}(\mathbf{r}, t) &= \mu_0 \hat{\phi} \int_{\rho_1}^{\rho_2} \int_0^{2\pi} \int_{-\infty}^{\infty} \\ &\quad \frac{1}{4\pi|\mathbf{r} - \mathbf{r}'|} J_\phi(\rho', z', t) \cos \phi' \rho' d\rho' d\phi' dz', \quad (35) \end{aligned}$$

where $\mathbf{A}^{\text{ind}}(\mathbf{r}, t)$ is axial-symmetric, $\hat{\phi}' = -\hat{x} \sin \phi' + \hat{y} \cos \phi'$, and in the x - z plane the Greens function $1/4\pi|\mathbf{r} - \mathbf{r}'|$ is even in ϕ' and $\hat{y} = \hat{\phi}$.

By inserting the free space Green's function expansion (5) into (35) and integrating over the ϕ' coordinate, the magnetic potential is given by

$$\begin{aligned} \mathbf{A}^{\text{ind}}(\mathbf{r}, t) &= \mu_0 \frac{i}{4} \hat{\phi} \int_{-\infty}^{\infty} \int_{\rho_1}^{\rho_2} \int_{-\infty}^{\infty} \\ &\quad J_1(i|\alpha|\rho) H_1^{(1)}(i|\alpha|\rho') J_\phi(\rho', z', t) e^{i\alpha(z-z')} \rho' d\rho' dz' d\alpha, \quad (36) \end{aligned}$$

where $\rho < \rho_1$, cf., section II-C for further details. Next, by inserting (12), (19) and (20) into the expression above, and integrating over the z' coordinate, the magnetic potential becomes

$$A_\phi^{\text{ind}}(\rho, z, t) = \mu_0^2 \left(\frac{i\pi}{2} \right)^2 \sigma \frac{\dot{z}_0(t)}{2\pi} ahM \int_{-\infty}^{\infty} i\alpha J_1(i|\alpha|\rho) J_1(i|\alpha|a) \frac{\sin(\alpha h/2)}{\alpha h/2} e^{i\alpha(z-z_0(t))} \int_{\rho_1}^{\rho_2} (H_1^{(1)}(i|\alpha|\rho'))^2 \rho' d\rho' d\alpha, \quad (37)$$

where the relation $\int_{-\infty}^{\infty} e^{i(\alpha-\alpha')z'} dz' = 2\pi\delta(\alpha-\alpha')$ has been used. The induced magnetic flux density at $\rho = a$ is given by

$$B_\rho^{\text{ind}}(a, z, t) = -\frac{\partial}{\partial z} A_\phi^{\text{ind}}(a, z, t) = \mu_0^2 \frac{\pi^2}{4} \sigma \frac{\dot{z}_0(t)}{2\pi} ahM \int_{-\infty}^{\infty} \alpha^2 |J_1(i|\alpha|a)|^2 \frac{\sin(\alpha h/2)}{\alpha h/2} e^{i\alpha(z-z_0(t))} \int_{\rho_1}^{\rho_2} (H_1^{(1)}(i|\alpha|\rho'))^2 \rho' d\rho' d\alpha. \quad (38)$$

The magnetic force acting on the magnet is given by the Lorentz force equation

$$\mathbf{F}^{\text{mag}} = \int_0^{2\pi} \int_{z_0(t)-h/2}^{z_0(t)+h/2} \mathbf{J}_s(\mathbf{r}) \times \mathbf{B}^{\text{ind}}(\mathbf{r}) dS, \quad (39)$$

and hence

$$F_z^{\text{mag}} = -M \int_0^{2\pi} \int_{z_0(t)-h/2}^{z_0(t)+h/2} B_\rho^{\text{ind}}(a, z, t) a d\phi dz = -2\pi Ma \int_{z_0(t)-h/2}^{z_0(t)+h/2} B_\rho^{\text{ind}}(a, z, t) dz. \quad (40)$$

By using

$$\int_{z_0(t)-h/2}^{z_0(t)+h/2} e^{i\alpha(z-z_0(t))} dz = h \frac{\sin(\alpha h/2)}{\alpha h/2}, \quad (41)$$

the final expression for the magnetic force is

$$F_z^{\text{mag}} = -\sigma M^2 \mu_0^2 C \dot{z}_0(t), \quad (42)$$

where C is the structure constant given by (29).

The equation of motion is obtained by applying Newton's second law

$$-\sigma M^2 \mu_0^2 C \dot{z}_0(t) - mg = m\ddot{z}_0(t), \quad (43)$$

which has the solution for $t \geq 0$

$$\begin{cases} z_0(t) = g\tau [\tau(1 - e^{-t/\tau}) - t], \\ \dot{z}_0(t) = g\tau [e^{-t/\tau} - 1], \\ \ddot{z}_0(t) = -ge^{-t/\tau}, \end{cases} \quad (44)$$

where the time constant τ is given by

$$\tau = \frac{m}{\sigma M^2 \mu_0^2 C}. \quad (45)$$

The stationary velocity is $v = -g\tau = -mg/(\sigma M^2 \mu_0^2 C)$, which is in agreement with (32).

III. EXPERIMENTAL VALIDATION AND ESTIMATION

Two neodymium permanent disc magnets of grade N45 and N42 have been tested together with two metal cylinders made of aluminum and copper. These measurement objects are referred to here as N45, N42, Al and Cu, respectively, and their structural parameters are listed in Table I.

Magnet	radius a [mm]	height h [mm]	mass m [g]
N45	15	20	107
N42	17.5	20	144
Cylinder	radius ρ_1 [mm]	radius ρ_2 [mm]	length L [mm]
Al	20	30	102
Cu	16.1	17.5	136

TABLE I
MAGNET AND CYLINDER DATA

The experiments have been conducted in three different test cases denoted by N45-Al, N42-Al and N45-Cu, and with the measurement cylinder in four different temperature scenarios: 1) cylinder heated with boiling water (+100° C) during a few minutes; 2) cylinder in room temperature (+23° C) for calibration; 3) cylinder cooled in a freezer (-20° C) for at least 8 hours and 4) cylinder cooled with liquid nitrogen (-196° C) during a few minutes. The experiments were recorded on video and the time required for the magnet to fall the distance $L-h$ through the cylinder was measured by time-stepping and visually inspecting the video. The resulting measured timing data in the four temperature scenarios are summarized in Table II.

Test case timing	+100° C t_1 [s]	+23° C t_2 [s]	-20° C t_3 [s]	-196° C t_4 [s]
N45-Al	0.90	1.10	1.30	3.85
N42-Al	1.43	1.73	2.05	5.98
N45-Cu	1.78	2.00	2.29	9.35

TABLE II
MEASURED TIMING DATA

The structure constant C is first calculated based on (29), and the magnetization M of the magnet is then identified by using (32) together with data (σ and v) corresponding to the calibration measurement at room temperature. Here, the conductivity data at different temperatures for aluminum and copper have been obtained from [8]. Once the magnetization M of the magnet has been identified, the induced current I_{ind} and the maximum magnetic flux density $B = B_z(0, 0)$ can be calculated from (33) and (15), respectively. The normalized integrands for computing C , I_{ind} and B are shown in Fig. 2 for the test case N45-Al. It has been shown in section II-D and II-F that these integrands are well behaved continuous functions that decay exponentially for large α . Hence, a simple numerical integration scheme is used here based on the composite Simpson's rule [4], and all the integrals evaluated in these examples converged to 4-5 digits based on $N = 1001$ sample points and an integration interval $[0, 1000]$. The resulting set of estimated parameters for the three test cases are summarized in Table III including the time constant τ given by (45).

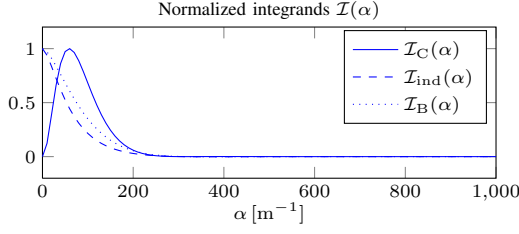


Fig. 2. Numerical integration for the test case N45-Al at calibration temperature $T = +23^\circ\text{C}$. The plots show the normalized integrands $\mathcal{I}_C(\alpha)$, $\mathcal{I}_{\text{ind}}(\alpha)$ and $\mathcal{I}_B(\alpha)$ in the numerical integration of C defined by (29), I_{ind} defined by (33), and $B_z(0,0)$ defined by (15), respectively.

Test case	C [mm ³]	M [kAm ⁻¹]	I_{ind} [A]	B [T]	τ [ms] at $+23^\circ\text{C}$
N45-Al	296	899	61	0.63	7.6
N42-Al	647	884	54	0.55	4.8
N45-Cu	193	1003	24	0.70	5.9

TABLE III
ESTIMATED PARAMETERS

A validation of the theory is obtained by considering the estimated values for M and B regarding the same magnet N45 obtained from the two test cases N45-Al and N45-Cu, as shown in Table III. In this case, the relative error is about 10%. It is also interesting to compare the equivalent current of the magnets $Mh \approx 18\text{-}20\text{ kA}$, with the corresponding induced current in the cylinders $I_{\text{ind}} \approx 20\text{-}60\text{ A}$. It is emphasized that the purpose of these measurements have been for illustration rather than for accurate parameter identification. Hence, an industrial application for accurate parameter identification would incorporate a much more controlled experiment with an elaborate device for timing measurements, etc.

Finally, it is illustrative to demonstrate an application of temperature (or resistivity/conductivity) measurements, and the fact that the resistivity of conductors is strongly dependent on the temperature. Hence, the temperature of the measurement cylinders in the four different temperature scenarios described above are estimated based on the calibrated magnetization M given in Table III. The timing data of Table II is used to determine the conductivity σ of the cylinder based on (32), and the corresponding resistivity $\rho = 1/\sigma$ is mapped to a temperature according to the material data given in [8]. The results are summarized in Table IV, and illustrated in Fig. 3 for the test case N45-Al. It is noted that the resistivity ρ of the cylinder, and hence the velocity v of the fall, are almost linear in the temperature T . As expected, the temperature estimations in the two test cases N45-Al and N42-Al are rather consistent, as the same aluminum cylinder is employed in both cases.

Test case temperature	+100°C T_1 [°C]	+23°C T_2 [°C]	-20°C T_3 [°C]	-196°C T_4 [°C]
N45-Al	76	23	-14	-145
N42-Al	73	23	-14	-144
N45-Cu	54	23	-8	-170

TABLE IV
ESTIMATED CYLINDER TEMPERATURES

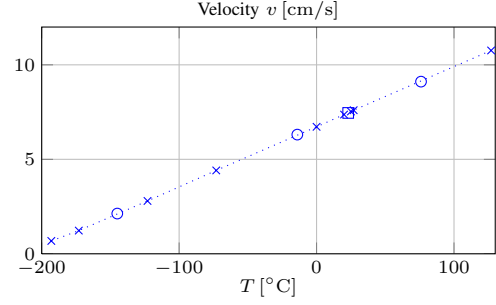


Fig. 3. Experimental results for the N45-Al test case: The velocity of the fall v vs. cylinder temperature T . The electromagnetic model is calibrated based on the measured timing data at $T = +23^\circ\text{C}$. The resistivity data for aluminum at different temperatures [8] (indicated with “x”) as well as the experimental data (indicated with “o”) are incorporated into the model.

IV. SUMMARY

A rigorous quasi-static electromagnetic theory has been presented for experiments and calibration of strong permanent magnets falling inside a metal cylinder. The results can be used by teachers and students in electromagnetics who wish to obtain a deeper insight into the analysis and experiments regarding this phenomenon. If the experiment is carefully controlled, the theoretical results could also be employed with industrial applications such as with an accurate calibration of strong permanent magnets.

APPENDIX A

EXPANSION OF THE FREE SPACE GREEN’S FUNCTION

The free space Green’s function for the scalar Helmholtz wave equation satisfies

$$\{\nabla^2 + k^2\} G(\mathbf{r}, \mathbf{r}') = -\delta(\mathbf{r} - \mathbf{r}'), \quad (46)$$

where k is the wavenumber of the free space and $\delta(\cdot)$ the three-dimensional Dirac delta function, cf., [7]. When the time-dependence is given by the factor $e^{-i\omega t}$, the Green’s function is given explicitly by the outgoing spherical wave

$$G(\mathbf{r}, \mathbf{r}') = \frac{e^{ik|\mathbf{r}-\mathbf{r}'|}}{4\pi|\mathbf{r}-\mathbf{r}'|}, \quad (47)$$

where $k = \omega/c$ and where ω is the angular frequency and c the speed of light in the free space. The Green’s function (47) can be expanded in cylindrical scalar wave functions as

$$\frac{e^{ik|\mathbf{r}-\mathbf{r}'|}}{4\pi|\mathbf{r}-\mathbf{r}'|} = \frac{i}{8\pi} \int_{-\infty}^{\infty} \sum_{m=-\infty}^{\infty} J_m(\kappa\rho_{<}) H_m^{(1)}(\kappa\rho_{>}) e^{im(\phi-\phi')} e^{i\alpha(z-z')} d\alpha, \quad (48)$$

where α is the Fourier variable corresponding to a Fourier transformation along the longitudinal coordinate z , and $J_m(\cdot)$ and $H_m^{(1)}(\cdot)$ are the regular Bessel functions and the Hankel functions of the first kind, both of order m , respectively, see e.g., [3, 7]. Here, the transverse wavenumber is defined by

$$\kappa = \sqrt{k^2 - \alpha^2}, \quad (49)$$

where the square root¹ $\kappa = \sqrt{w}$ is defined such that $0 < \arg w \leq 2\pi$ and $0 < \arg \kappa \leq \pi$ and hence $\text{Im } \kappa \geq 0$. The arguments of the cylindrical functions above are furthermore defined by $\rho_{<} = \min\{\rho, \rho'\}$ and $\rho_{>} = \max\{\rho, \rho'\}$, and where the primed variables represent the source point and the unprimed variables represent the field point. It is noted that the expansion in (48) involves regular Bessel functions $J_m(\kappa\rho)$ for $\rho < \rho'$ and outgoing (radiating) Hankel functions $H_m^{(1)}(\kappa\rho)$ for $\rho > \rho'$. It is also noted that the combination $J_m(\kappa\rho_{<})H_m^{(1)}(\kappa\rho_{>})$ is continuous across the point where $\rho = \rho'$ with its value $J_m(\kappa\rho')H_m^{(1)}(\kappa\rho')$.

To verify that the expansion in (48) satisfies (46), it is first noted that the cylindrical scalar wave functions $\psi_m(\kappa\rho)e^{im\phi}e^{i\alpha z}$ satisfy the homogeneous Helmholtz wave equation

$$\{\nabla^2 + k^2\} \psi_m(\kappa\rho)e^{im\phi}e^{i\alpha z} = 0, \quad (50)$$

where $\psi_m(\kappa\rho)$ is any cylindrical function of order m satisfying the Bessel differential equation [1, 7, 9]

$$\left\{ \frac{1}{\rho} \frac{\partial}{\partial \rho} \rho \frac{\partial}{\partial \rho} + \kappa^2 - \frac{m^2}{\rho^2} \right\} \psi_m(\kappa\rho) = 0. \quad (51)$$

Consider now the distributional relationship (46) in cylindrical coordinates

$$\begin{aligned} \left\{ \frac{1}{\rho} \frac{\partial}{\partial \rho} \rho \frac{\partial}{\partial \rho} + \frac{1}{\rho^2} \frac{\partial^2}{\partial \phi^2} + \frac{\partial^2}{\partial z^2} + k^2 \right\} G(\rho, \phi, z, \rho', \phi', z') \\ = -\frac{1}{\rho} \delta(\rho - \rho') \delta(\phi - \phi') \delta(z - z'). \end{aligned} \quad (52)$$

Take the Fourier transform of (52) to yield

$$\begin{aligned} \left\{ \frac{1}{\rho} \frac{\partial}{\partial \rho} \rho \frac{\partial}{\partial \rho} - \frac{m^2}{\rho^2} - \alpha^2 + k^2 \right\} G_m(\rho, \alpha, \rho', \phi', z') \\ = -\frac{1}{\rho} \delta(\rho - \rho') \frac{1}{2\pi} e^{-im\phi'} e^{-i\alpha z'}, \end{aligned} \quad (53)$$

where the following relationships have been used $\frac{\partial}{\partial \phi} \leftrightarrow im$, $\frac{\partial}{\partial z} \leftrightarrow i\alpha$, $\sum_m e^{im(\phi - \phi')} = 2\pi \delta(\phi - \phi')$ and $\int e^{i\alpha(z - z')} d\alpha = 2\pi \delta(z - z')$.

From (48), it follows that the conjecture is

$$G_m(\rho, \alpha, \rho', \phi', z') = \frac{i}{4} J_m(\kappa\rho_{<}) H_m^{(1)}(\kappa\rho_{>}) e^{-im\phi'} e^{-i\alpha z'}, \quad (54)$$

and it will now be verified that (54) satisfies the distributional relationship (53). Hence, by inserting (54) into (53), it follows that

$$\begin{aligned} \left\{ \frac{1}{\rho} \frac{\partial}{\partial \rho} \rho \frac{\partial}{\partial \rho} - \frac{m^2}{\rho^2} - \alpha^2 + k^2 \right\} J_m(\kappa\rho_{<}) H_m^{(1)}(\kappa\rho_{>}) \\ = i \frac{2}{\pi} \frac{1}{\rho} \delta(\rho - \rho'). \end{aligned} \quad (55)$$

It is noted that $J_m(\kappa\rho_{<})H_m^{(1)}(\kappa\rho_{>})$ is a continuous function across $\rho = \rho'$, and with a discontinuous derivative. Hence, by

applying to (55) the integration $\int_{\rho' -}^{\rho' +} \{\cdot\} \rho d\rho$ it follows that

$$\left[\rho \frac{\partial}{\partial \rho} J_m(\kappa\rho_{<}) H_m^{(1)}(\kappa\rho_{>}) \right]_{\rho' -}^{\rho' +} = i \frac{2}{\pi}, \quad (56)$$

where $\rho' +$ and $\rho' -$ means taking a limit towards ρ' from above and from below, respectively. It follows that

$$\kappa\rho' \left[J_m(\kappa\rho') H_m^{(1)'}(\kappa\rho') - J_m'(\kappa\rho') H_m^{(1)}(\kappa\rho') \right] = i \frac{2}{\pi}, \quad (57)$$

where $J_m'(\cdot)$ and $H_m^{(1)'}(\cdot)$ denote a differentiation with respect to the argument. The validity of (57), and hence of (53), is finally verified by using the Wronskian relation $\mathcal{W}(J_m(\zeta), H_m^{(1)}(\zeta)) = 2i/(\pi\zeta)$, cf., [1, 9].

The analysis and results given above are also valid when $k = 0$, and the expansion used in (5) is hence given by (48) with $\kappa = i|\alpha|$.

REFERENCES

- [1] G. B. Arfken, H. J. Weber, and F. E. Harris. *Mathematical Methods for Physicists*. Academic Press, New York, seventh edition, 2013.
- [2] D. K. Cheng. *Field and wave electromagnetics*. Addison-Wesley, Reading, MA, USA, 1989.
- [3] R. E. Collin. *Field Theory of Guided Waves*. IEEE Press, New York, second edition, 1991.
- [4] G. Dahlquist and Å. Björck. *Numerical methods*. Prentice-Hall, Inc., Englewood Cliffs, New Jersey, 1974.
- [5] J. Fraden. *Handbook of Modern Sensors: Physics, Designs, and Applications*. Springer, USA, fourth edition, 2010.
- [6] D. J. Griffiths. *Introduction to Electrodynamics*. Prentice-Hall, Inc., Englewood Cliffs, New Jersey, third edition, 1999.
- [7] J. D. Jackson. *Classical Electrodynamics*. John Wiley & Sons, New York, third edition, 1999.
- [8] D. R. Lide. *CRC handbook of chemistry and physics : a ready-reference book of chemical and physical data*. Ed. 88 (2007-2008). CRC Press, Boca Raton, Florida, 2008.
- [9] F. W. J. Olver, D. W. Lozier, R. F. Boisvert, and C. W. Clark. *NIST Handbook of mathematical functions*. Cambridge University Press, New York, 2010.
- [10] G. N. Watson. *A Treatise on the Theory of Bessel Functions*. Cambridge University Press, Cambridge, U.K., second edition, 1966.
- [11] A. H. Zemanian. *Distribution theory and transform analysis: an introduction to generalized functions, with applications*. McGraw-Hill, New York, 1965.

Sven Nordebo received the M.S. degree in electrical engineering from the Royal Institute of Technology, Stockholm, Sweden, in 1989, and the Ph.D. degree in signal processing from Luleå University of Technology, Luleå, Sweden, in 1995. Since 2002 he is a Professor of Signal Processing at the Department of Physics and Electrical Engineering, Linnæus University. His research interests are in statistical signal processing, electromagnetic wave propagation, inverse problems and imaging.

Alexander Gustafsson received the M.S. degree in physics from the Linnæus University, Växjö, Sweden, in 2011. Since 2013 he is a Ph.D student in physics at the Department of Physics and Electrical Engineering, Linnæus University. His research interests are in molecular dynamics on surfaces.

¹If the square root is defined as e.g., with the MATLAB software where $-\pi/2 < \arg \sqrt{w} \leq \pi/2$ for $-\pi < \arg w \leq \pi$, then κ can be defined here as $\kappa = i\sqrt{-k^2 + \alpha^2}$ which implies that $0 < \arg \kappa \leq \pi$.